Nanoindentation studies of oxide aluminum-chrome carbide composite coating

Maksim Kireitseu
Department of Mechanics and Mechanics and Tribology
Institute of Machine Reliability (INDMASH), National Academy of Sciences of Belarus
Lesnoe 19 - 62, Minsk 223052, Belarus e-mail: indmash@rambler.ru

The work revealed the possibility to improve physical, mechanical properties of oxide aluminum-based layers by CrC-based nanoparticles produced by the metalorganic chemical vapor deposition. Oxide aluminum layer is formed on aluminum parts by micro arc oxidizing technology or electroplating deposition. It is found to be high microhardness and fracture resistance regarding initiation and propagation of Palmquist cracks during indentation. CrC-based layer exhibited a dense and columnar microstructure. Nanoindentation test showed high hardness for oxide aluminum-CrC-based multilayed composite coating and almost homogeneous oxide aluminum layer in the range of 18-26 GPa. CrC-based layer filled the defects and pores might enhance crack propagation under overloaded indenter. For both series of the samples, fracture toughness was lower for the multilayed composite coating than that of the corresponding homogeneous oxide aluminum. As a whole, oxide aluminum-CrC-based multilayed composite coating exhibits higher scratch wear resistance compared to the oxide aluminum layer.

For more information, contact:
Dr. Maksim V. Kireitseu
Department of Mechanics and Tribology
Institute of Mechanics and Machine Reliability (INDMASH)
Lesnoe 19 - 62, Minsk 223052,
Belarus
Email: indmash@rambler.ru

Introduction

At the macro-scale, mechanical testing of thin coatings and multilayered composites composed of compliant multiphase materials, such as oxide aluminum, is often difficult, as coatings are difficult to grip and susceptible to creep ratcheting and other undesirable mechanical responses. Moreover, many applications such as packaging, turbine blades and gas-filled bladders involve bi-axial stresses, a stress state which is difficult to impose experimentally[1].

Indentation of oxide aluminum-CrC-based multilayed composite coating offers an interesting results of its mechanical response to conventional tension experiments, as the coating samples are easier to mount and the configuration naturally limits displacements and eliminates many of the problems associated with conventional uniaxial testing.

In this paper, we limit our attention to frictionless contact with an indenter. The non-linearity associated with solving large strain, large-deformation problems is dealt with in the context of non-linear differential equations, for which efficient numerical schemes abound. The calculations presented here illustrate that, in spite of some brief algebraic complexity, one can rapidly predict the mechanical response of coatings loaded transversely with an indenter, accounting fully for both large deformation effects and the details in the contact zone. A key result is that the analyses often produce simple, closed-form, power-law relationships that can be exploited to quickly convert experimentally measured load-displacement curves to mechanical properties.

There is a rather significant body of literature on the mechanics of large-deformation problems, an overview[2,3]. Much of the literature is concerned with point loading of composites or plates[1-4] and the inflation of initially flat or hemi-spherical caps, i.e. bulge testing[5-10]. While such previous efforts serve as useful background for the present work, they do not explicitly address the contact between a finite-sized indenter and the oxide aluminum composite.

However, there is an industrial interest in coatings with further improved wear resistance, hardness, and fracture toughness, for example, compared to CrC or BN single coatings. Multilayered coating structures such as superlattices, or nano-structured multilayers, where the individual layers may have a thickness in the nm range, is an emerging class of new hard protective coatings. Oxide aluminum matrix super lattices and multilayers of different oxides and carbides micro and nanostructures, e.g., oxide aluminum-CrC, are of interest due to the possibility of enhancing the hardness, wear resistance and overall performance compared to single-layered CrC layer or oxide aluminum coating. Enhanced hardness has been reported for oxide aluminum matrixes with alpha and gamma phases of oxide aluminum in the structure, both for single-crystal superlattices[11] as well as for polycrystalline nanostructured multilayers.[12]

In polycrystalline oxide aluminum matrix, high hardness is explained by the presence of dislocation between the layer interfaces. The dislocations are resulted from the difference in the shear module of the materials and coherency strains for small periodicity superlattices with significant lattice mismatch between the layers. In addition, mechanical properties are affected by the presence of grain boundaries and defects within the oxide aluminum layer. Typical micro arc oxidizing uses high current densities (up to 40 A/dm^2) when oxide aluminum layer is growing up at the substrate[13]. These conditions could induce large defects, micro voids and pores[14]. The layer consist of the principal phases of oxide aluminum[15]. A few works have been done on polycrystalline multilayered oxide aluminum films on common automobile parts from aluminum or its alloys.

The objective of the paper is to investigate the possibility to improve physical and mechanical properties of oxide aluminum-based ceramic composite by CrC-based nanoparticles produced by the metal organic chemical vapor deposition. Indentation technique will be used as perfect tool for characterizing the performance and durability of the composite. In addition, the mechanical properties of the coatings are discussed with respect to the phase composition.

Experimental materials and technique

The combination of an AFM and a nanoindenter (for example, MicroSystems, UK) is a further de-

velopment of the traditional Vickers microhardness testing device. This instrument allows for two measurement modes. It provides a surface topography of constant contact force in AFM mode and a force displacement curve in nanoindentation mode using the same tip. This feature provides a high spatial resolution to position the tip on the microstructure of interest. The sample is mounted on a scanner that allows for a movement in the plane normal to the axial motion of the tip. The transducer consists of a three-plate capacitor on whose central plate a tetrahedral diamond Berkovich-tip is mounted. A nanoindentation curve consists of a loading phase where the tip is pressed into the material up to a maximal force, a holding period where the tip creeps into the material and an unloading phase where the force on the material is released. The loading and holding phases result in both plastic and elastic deformation that cannot be distinguished. The unloading phase shows the elastic recovery of the material while the load is released. For isotropic elastic materials, the following relationship based on the analytical solution[16,17] for indenters of revolution:

$$S = \frac{2}{\sqrt{\pi}} \cdot \frac{E}{1-\nu^2} \sqrt{A_c} \qquad (1)$$

where S(hmax) describes the derivative of the unloading part at the point of initial unloading and Achmax the contact area, over which the material and the indenter are in contact at that position and time.

This variable contains Young's modulus and Poisson's ratio. Often, Poisson's ratio is assumed to be v = 0.26 for oxide aluminum, but we prefer to report indentation moduli to avoid this assumption. For the purpose of comparison, Young's modulus calculated for v = 0.26 is approximately 93% of the indentation modulus.

The unloading part allows determining elastic modulus and hardness. A second mechanical property can be calculated from the nanoindentation curve: hardness. The hardness was calculated from the first 50% of the second unloading segment using the Pharr and Oliver method.7,8 This variable describes the mean pressure the material can resist and is defined by the ratio of maximum load P over the contact area:

$$H = \frac{P_{\max}}{} \qquad (4)$$

The stress field imposed by the indentation process is heterogeneous and leads to plastic deformation around the tip. To achieve reproducible measurements, the average roughness of the sample in the contact area should be well below the applied indentation depth. The minimal distance between neighbor indents was set to approximately 3 times the contact diameter (i.e. =18 h for a Berkovich tip geometry).

Specimen preparation and measurements

The 5054 aluminum alloy as referred by the MIL specifications was the substrate on which oxide ceramic layers were produced by micro arc oxidizing. The thickness of the oxide aluminum layer is 250 μm, its microhardness is up to 18 GPa and its Young's modulus is 290 GPa.

The pyrolysis technology allows deposition of CrC particles that form hard CrC layers with low residual stresses. The pores and defects of alumina layer were filled by the CrC particles (see indexes on fig. 2). The pyrolitic deposition process was performed by the pyrolysis of a metal-organic liquid (Barhos) of Cr-organic compounds under vacuum in pressure range 4-8 Pa. The principal pieces of equipment are a vertical quartz tube reactor, a feeder of the liquid composed of the Cr-organic compounds and two cylinder furnaces located inside the internal space of the reactor. The reactor is connected with a vacuum pump through an entrainment separator. The chromium-organic liquid is fed into the upper furnace and evaporates in its inner volume. Vapors of the chromium-organic compounds are then delivered to the substrates placed on a special holder inside the lower furnace, where they decompose forming a coating. The deposition was performed under a pressure 2-14 Pa and a temperature of 430-450°C, which was measured by the W-Re thermocouple with the deviation of ±5°. The thickness of the CrC

layer ranges from 10 to 50 μm, its microhardness is 17GPa and its Young's modulus is 300 GPa.

The nanoindentation response of the oxide aluminum-CrC nanoparticles multilayer and homogeneous oxide aluminum coatings were determined using a NanoIndentory II instrument. The measurement procedure was as follows: load to maximum, unload to 10% of maximum load, hold for 50 s, load to maximum, hold for 200 s, and completely unload. The maximum load was 10 or 50 mN and a maximum of ten indents sequences were used for each maximum load. The data from the first hold segment ~50 s was used to correct the load-displacement data for thermal drift. The triangular Berkovich diamond indentor tip was calibrated following the procedure described in Ref. [18, 19].

After AFM and nanoindentation studies the sample was first scanned in AFM-mode. The topography measurement helped to characterize the polishing quality and to choose precisely the region of interest. The piezoelectric scanner of the AFM allows for a higher positioning accuracy than the x-y translation table that equips nanoindentation devices relying on optical microscopy.

Results

Electrochemical studies of the coating revealed that the coating is almost dense and porous-free. The Auger spectra were obtained at different values of the sputtering time. The results indicated the not uniform distribution of the substrate components when varying the coating thickness. It is supposed that the Al and O particles observed in the coating is the effect of diffusion between the substrate components and the CrC coating during the deposition at temperature above 400°C.

Figure 1 show the typical structure of oxide aluminum layer. The pores are shown on surface. Figure 2 shows that the CrC nanoparticles deposited on oxide aluminum-based ceramic layer fill the pores and other defects of the layer. The CrC nanoparticles and CrC coating have high adhesion to the oxide aluminum substrate since no exfoliation is visible in the fracture of the coated specimens at applied technological regimes. The coating is characterized by a fine-grained globule-like structure. It should be pointed out that one structure could consist of several grains, CrC nanoparticles or subgrains, therefore the size of CrC nanoparticle is smaller than the pore width.

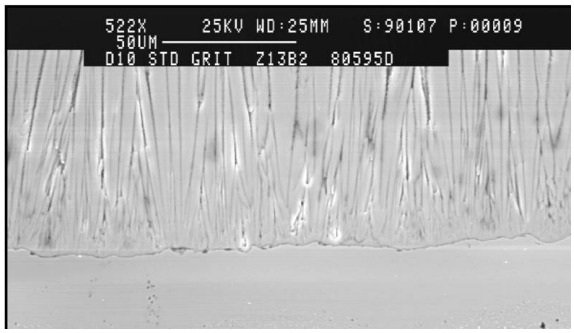

Figure 1. Microstructure of oxide aluminum-based nanostructured composite

The X-ray analysis revealed that the CrC top coating consists generally chromium carbides (Cr3C2 and Cr7C3). The coating heals various surface defects, pores and voids on the oxide aluminum surface (see fig. 2), which was deeply determined by studying the coating-substrate interface with the aid of SEM.

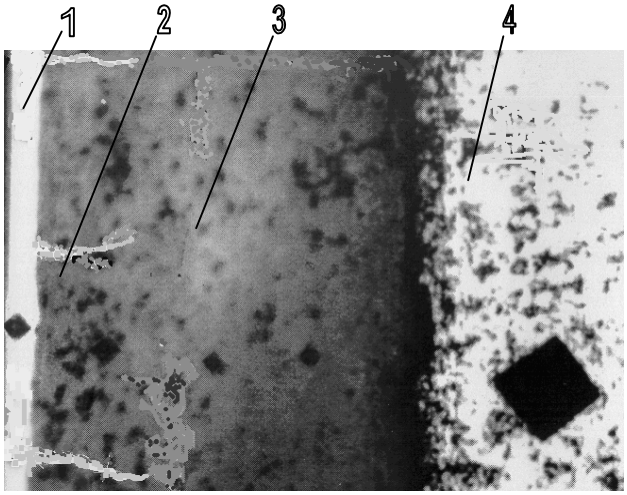

Figure 2. Microstructure of Al-Al2O3-CrC nanoparticles composite

The electrochemical studies and the SEM investigations revealed that the oxide aluminum-CrC composite coating is very dense and virtually defect-free. The healing resulted by CrC nanoparticles that fill most defects of oxide aluminum structure. The single oxide aluminum layer is formed; the failure is initiated by "opening" defects of the oxide aluminum structure. It results in reduced fracture resistance of

the oxide aluminum against initiation and propagation of micro and nanocracks through defects and pores.

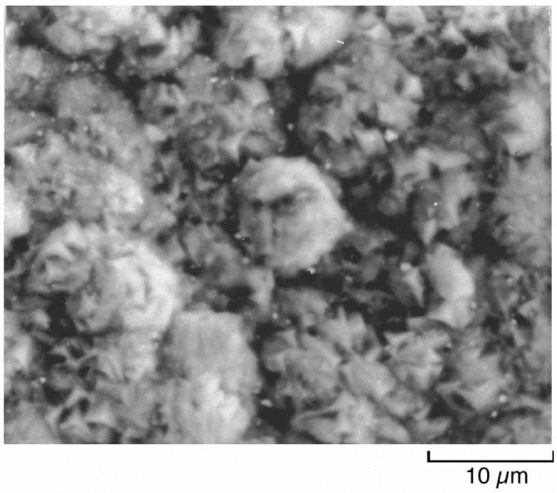

Figure 3.Topography of composite surface in AFM-mode

Nanoindentation

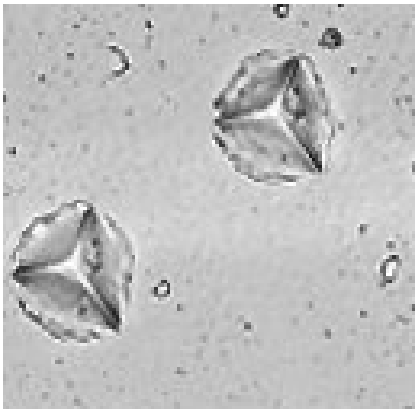

Figure 4. Indentation track.

Figure 4 shows Vickers indentations obtained on the surface of the coated and uncoated ceramic specimens. It is found that, whereas typical Palmquist cracks appear after the indentation of the uncoated specimen, there are not cracks near the corners of the Vickers indentation on the surface of the coated ceramic specimen.

Figure 5 shows nanoindentation load-displacement curves from oxide aluminum-CrC multilayer composite used for evaluating composite hardness. The initial loading segment contains an elastic-plastic displacement. The first unloading curve and the second loading curve differ substantially and form a hysteresis loop with a larger displacement during unloading than loading. The data from the first hold segment was used for correction of the load-displacement data for thermal drift and the second for investigating creep like dislocation nucleation and glide plastic behavior. Approximately 5-8 nm maximum load creep occurred at the maximum load hold segment in Fig. 5.

For all oxide aluminum-CrC composites, the maximum displacement was 270-280 nm that is lower then that of single oxide aluminum layer. The first and the second unloading curves from these composites show the same elastic behavior with small creep. However, the elastic response from the films differs and thus results in the different apparent hardness. Single oxide aluminum layer exhibited the largest percentage of elastic recovery from maximum displacement during the second unloading.

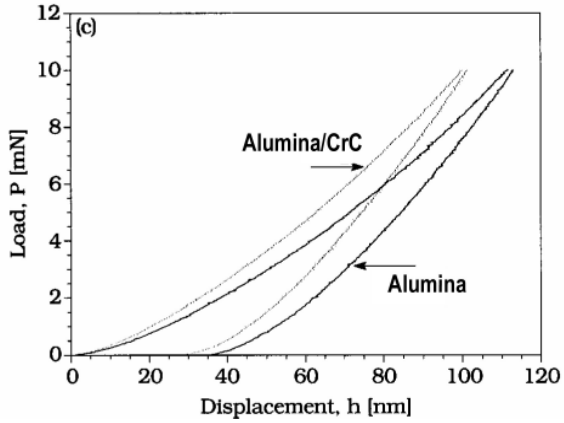

Figure 5. Nanoindentation curves.

The hardnesses of the oxide aluminum layers were in the range of published nanoindentation hardness data between 18 and 26 GPa, depending on film microstructure and hardness evaluation procedure. The hardnesses of the oxide aluminum-CrC composite were in the range of data between 20 and 28 GPa, depending on film microstructure, thickness of the layers and hardness evaluation procedure.

Discussion

The combination of AFM and nanoindentation has proven to be a powerful tool to provide reliable micromechanical properties of the oxide aluminum-CrC nanoparticles composite. The strong advantage

of the available AFM-mode over the conventional nanoindentation technique lies in the possibility to select the location of the indentations within a few tenths of nanometers and to quantify the sample's surface topography, hence the quality of the sample preparation.

The higher standard deviations found in previous nanoindentation studies were probably associated with averaging over multiple samples. The results indicated that, in first approximation, the composite might be seen as a nanoassembly of nanostructural units with distinct mechanical properties between them but rather homogeneous properties within the same nanostructured elements. This finding has potentially important implications in the process of fracture propagation that is clearly related to composite structure and heterogeneity.

The major limitation of the nanoindentation data analysis remains the hypothesis of isotropy of the tested material. In fact, the indentation curve depends to a widely unknown extent on all anisotropic elastic constants of the tested material. Since the oxide aluminum-CrC nanostructured composite and most probably also the oxide aluminum layer is elastically anisotropic, the reported results are some weighted average of the elastic moduli along the various material orientations.

Large compressive residual stresses arise from energetic metalorganic deposition of CrC nanoparticles healing defects of oxide aluminum structure were found in the films. The stresses were higher in the thicker CrC layers due to the higher nanoparticle energy that creates internal stresses over a more extended region that subsequently becomes buried under the growth front.

Conclusion

The coating deposited with the aid of MOCVD on oxide aluminum ceramics, which is composed of a mixture of Cr and chromium carbides, has good microhardness as high as 20 GPa, fracture resistance and adhesion to the oxide ceramic substrate due to a high rate of its chemical and structural interaction with the oxide aluminum substrate when depositing.

The CrC nanoparticles leads to healing various surface defects and pores of oxide aluminum and retardation of the crack initiation and its propagation in the near-surface composite. It results in enhanced transverse rupture strength, fracture toughness, and microhardness of the coated oxide aluminum ceramic specimens. The damage in the Al_2O_3-CrC composite is suppressed, in contrast to that in the single oxide aluminum. CrC nanoparticles and clusters deflect corresponding to deformation plastic material flow. Deformation takes place in result of radial spreading of contact zone under indenter with initiating of local cracks. The degree of toughening associated with crack healing is determined by the number of healing defects and the effectiveness of the individual healing.

References

1. Fulton, J.P. and Simmonds, J.G. Large deformations under vertical edge loads of annular membranes with various strain energy densities, International Journal of Non-Linear Mechanics, 21, 257-267 (1986).
2. Hong, S. Weihs, T.P., Bravman, J.C. and Nix, W.D. Measuring stiffnesses and residual stress of silicon nitride thin films, Journal of Electronic Materials, 19, 903-909 (1990).
3. Li, X. and Steigmann, D.J. Point loads on a hemispherical elastic membrane, International Journal of Non-Linear Mechanics, 34, 569-581 (1995).
4. Libai, A. and Simmonds, J.G. The Nonlinear Theory of Elastic Shells, 2nd ed., Cambridge University Press, Cambridge, U.K (1998).
5. Yang, W.H. and Feng, W.W. On axisymmetrical deformations of nonlinear membranes, Journal of Applied Mechanics, 34, 1002-1011 (1970).
6. Yang, W.H. and Hsu, K.H. Indentation of a circular membrane, Journal of Applied Mechanics, 36, 227-230 (1971).
7. Tsakalakos, T. The bulge test: a comparison of theory and experiment for isotropic and anisotropic films, Thin Solid Films, 75, 293-305 (1981).
8. Small, M.K. and Nix, W.D. Analysis of the accuracy of the bulge test in determining the mechanical properties of thin films, Journal of Materials Research, 7, 1553-1563 (1992).
9. Vlassak, J.J. and Nix, W.D. A new bulge test technique for the determination of

Young's modulus and Poisson's ratio of thin films, Journal of Materials Research, 7, 3242-3249 (1992).
10. Poilane, C., Delobell, P., Lexcellent, C., Hayashi, S. and Tobushi, H. Analysis of the mechanical behavior of shape memory polymer deflection tests, Thin Solid Films, 379, 156-165 (1999).
11. B. Bhushan and B. K. Gupta, Handbook of Tribology ~McGraw-Hill, New York, 1991, 4, 57.
12. M. Shinn, L. Hultman, and S. A. Barnett, J. Mater. Res. 7, 901, 1992.
13. X. Chu, M.S. Wong, W.D. Sproul, S.L. Rhode, and S.A. Barnett, J.Vac.Sci.Technol. A10,1604, 1992.
14. K. H. Muller, Phys. Rev. B 35, 7906, 1987.
15. H. Ljungcrantz, L. Hultman, J.-E. Sundgren, and L. Karlsson, J. Appl. Phys. 78, 832, 1995.
16. M. S. Wong, W. D. Sproul, X. Chu, and S. A. Barnett, J. Vac. Sci. Technol. A 11, 1528, 1993.
17. G. M. Pharr, W. C. Oliver, and F. R. Brotzen, J. Mater. Res. 7, 613, 1992.
18. W. C. Oliver and G. M. Pharr, J. Mater. Res. 7, 1564, 1992.
19. W. C. Oliver, C. J. McHargue, and S. J. Zinkle, Thin Solid Films 153, 185, 1987.
20. B. Lawn, Fracture of Brittle Solids. Cambridge University Press, Cambridge, 1993.
21. R.W. Hertzberg, Deformation and Fracture Mechanics of Engineering Materials. - Wiley, NY, 1976, p. 11.

